

Communication

Evaluation of Leaf Chlorophyll Content from Acousto-Optic Hyperspectral Data: A Multi-Crop Study

Anastasia Zolotukhina ^{1,2,*}, Alexander Machikhin ¹, Anastasia Guryleva ^{1,2}, Valeria Gresis ^{2,3}, Anastasia Kharchenko ³, Karina Dekhkanova ³, Sofia Polyakova ⁴, Denis Fomin ^{2,4}, Georgiy Nesterov ² and Vitold Pozhar ^{1,2}

¹ Acousto-Optic Spectroscopy Laboratory, Scientific and Technological Centre of Unique Instrumentation, Russian Academy of Sciences, 15 Butlerova, 117342 Moscow, Russia; machikhin@ntcup.ru (A.M.); guryleva@bmstu.ru (A.G.); vitold@ntcup.ru (V.P.)

² Laser and Optical-Electronic Systems Department, Bauman Moscow State Technical University (National Research University), 52nd Baumanskaya, 105005 Moscow, Russia; gresis-vo@rudn.ru (V.G.); nesterovgeorgiyv@yandex.com (G.N.)

³ Agrarian Technological Institute, People's Friendship University of Russia, 117198 Moscow, Russia; kharchenko_ak@pfur.ru (A.K.); dehkanovakr@mail.ru (K.D.)

⁴ Perm Agricultural Research Institute, Division of Perm Federal Research Center Ural Branch of Russian Academy of Sciences, 614532 Perm, Russia; ss.polyakova@yandex.ru

* Correspondence: zolotukhina.aa@ntcup.ru



Citation: Zolotukhina, A.; Machikhin, A.; Guryleva, A.; Gresis, V.; Kharchenko, A.; Dekhkanova, K.; Polyakova, S.; Fomin, D.; Nesterov, G.; Pozhar, V. Evaluation of Leaf Chlorophyll Content from Acousto-Optic Hyperspectral Data: A Multi-Crop Study. *Remote Sens.* **2024**, *16*, 1073. <https://doi.org/10.3390/rs16061073>

Academic Editors: Chein-I Chang, Shengwei Zhong, Shuhan Chen and Akira Iwasaki

Received: 3 February 2024

Revised: 4 March 2024

Accepted: 15 March 2024

Published: 18 March 2024



Copyright: © 2024 by the authors. Licensee MDPI, Basel, Switzerland. This article is an open access article distributed under the terms and conditions of the Creative Commons Attribution (CC BY) license (<https://creativecommons.org/licenses/by/4.0/>).

1. Introduction

Sustainable intensification of agriculture is a reasonable concept in food production to meet dramatically surging demand [1], which by most estimates could at least double by 2050 [2]. This approach aims to increase agricultural production combined with reduced degradation of the environment or even the restoration of ecosystem functioning. To overcome this challenge, precision agriculture (PA) is one of the promising strategies. In addition to innovative farm machinery, it manages agricultural operations in a flexible, applicable and timely manner to balance yields and negative environmental impacts [3]. For optimal plant growth, PA adapts the use of fertilizers, pesticides, irrigation and tillage

to the variability and uncertainty in agricultural systems. PA decision making involves the collection of advanced information on crop health and soil state and subsequent data analysis [4].

Chlorophyll (Chl) is an essential light-absorbing leaf pigment crucial for plant growth and development, as it is involved in photosynthesis and influences the cycling of nutrients, nitrogen, carbon and water [5]. Thus, Chl content (CC) is a valuable measure of plant health and an important part of PA. It helps to monitor and assess physical and chemical plant stresses such as water, light and nutrition deficiencies, detect diseases and weeds and solve many other tasks [6–8]. Various CC estimation techniques are applicable depending on the task (Figure 1).

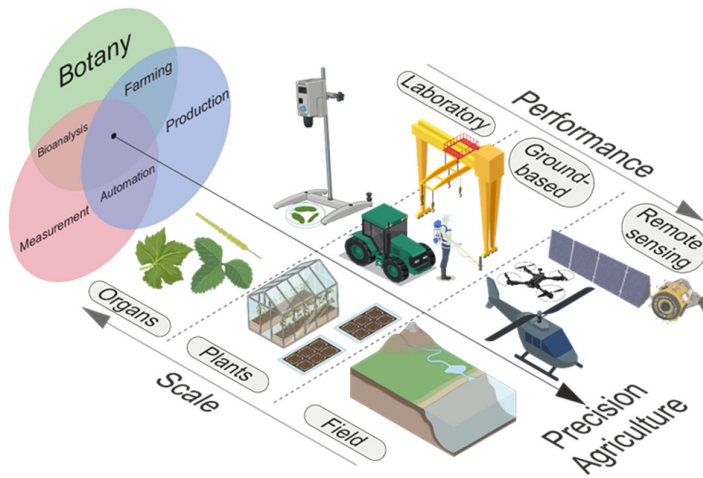


Figure 1. CC estimation procedures within PA concept.

Well-proven and accurate laboratory methods such as chromatography and spectrophotometry are widely used to evaluate CC in leaves. These methods require consumables and are time-consuming and hence are inapplicable to inspecting large areas. CC estimation by field deployable systems is primarily based on fluorimetry, colorimetry or spectroscopy [9,10]. It enables remote non-destructive monitoring of individual crops but is barely suitable for large-scale field diagnostics with high temporal or spatial resolution.

Another technology for CC mapping involves a well-established combination of remote sensing and spectral imagery [11]. It is based on reflectance spectroscopy and allows CC mapping over large areas [12]. The performance of such hyperspectral imaging (HSI) systems depends on their physical principle [13]. High-throughput and relatively affordable devices are mainly snapshot systems and acquire spectral images in just a few narrow bands. The selection of bands depends on specific application and observation conditions and is a key factor in terms of CC evaluation accuracy.

The relationship between spectral data and pigment content enables identification of empirical (index-based approach), analytical (radiative transfer model inversion) and hybrid techniques. Utilizing inversion techniques on renowned models like PROSPECT [14], SAIL [15], PROSAIL [16] and three-dimensional models [17] is extensively employed in CC evaluation methods. There are also hybrid techniques that merge the benefits of using radiative transfer models for training with machine learning [18]. However, applying radiative transfer model inversion to hyperspectral data on a per-pixel basis requires substantial computational resources [19], while simpler index-based methods currently achieve accuracy comparable to hybrid approaches [20,21].

Within an index-based approach, wavelengths sensitive to CC have to be specified [22]. The main issue that hampers CC measurement is that the reflected spectrum is a combination of multiple pigments and biochemical contents, textural, morphological and structural properties, leaf orientation, viewing and illumination geometry, atmospheric and topographic effects, etc. [23]. To overcome and/or minimize these effects, numerous Chl indices

(CIs) have been introduced. They are necessary to convert spectral reflectivity measured at a few wavelengths to CC value [24]. Currently, more than 10 CIs have already been applied, and none of them have become common and dominating for in-field CC mapping. Thus, selection of the most suitable CI is a primary task for CC evaluation. In practice, it means that it is necessary to calculate multiple CIs, build CC models based on every index [25–27] and define the best one in terms of fitting accuracy [28]. Therefore, acquired HSI data have to contain images at all wavelengths involved in the CIs to be calculated.

Acousto-optical (AO) imagers seem very attractive for calculating CIs and CC assessment due to their agility and rapid random-spectral-access tuning. This feature reduces the data redundancy and increases data acquisition and processing speed as well as monitoring performance [25]. In comparison to other spectral-scanning principles (Fabry–Perot, liquid crystals, etc.), AO tunable filters (AOTFs) deliver a unique combination of tuning time and spatial and spectral resolution. Moreover, successful implementation of in-field crop monitoring by AOTF-based HSI systems has been already demonstrated [26,27,29].

The vast majority of reported studies on remote CC mapping introduce CI-based models calculated from single-crop data. A robust approach to CI selection for multiple vegetation types is still an open issue. A multi-crop model is promising in terms of resistance to a variety of canopy structures and ease of practical use and data processing.

In [30], we conducted a single-crop (soybean) study and demonstrated the feasibility of AO imagery for CC measurements in laboratory conditions. This study is a significant step forward towards field measurements. In practice, we usually almost never see a uniform field filled with a single crop. At least, weeds or other varieties may be present. This is one of the reasons why it is important to define the spectral index and regression model properly, i.e., with respect to the features specific for a particular field. In this study, we chose crops that differ greatly in biophysical properties and chlorophyll content in order to show that even in this case the proper index and regression model may be found using an AO imaging system. For 90 inspected samples of plant leaves, the optimal vegetation index and linear regression model were found. The results of this study demonstrate that AOTF-based imagers show great promise for fast CC mapping and other laboratory spectral-index-related measurements, which are highly important in various PA tasks.

2. Materials and Methods

2.1. Experimental Plants

To build sustainable CI-based CC model, six plants with various morphological, structural and biochemical leaf properties and typical CC were selected: hibiscus (*Hibiscus rosa-sinensis*), birch (*Betula populifolia*), bird-cherry tree (*Ribes rubrum*), black currant (*Prunus padus*), barley (*Hordeum vulgare*) and wheat (*Triticum aestivum*). The leaves of all selected crops are of simple type, green from light to dark with bald laminas and have simple leaves blades, i.e., lobed or unlobed but not separated into leaflets with gage of leaf blade in the range of 180–230 µm [28,31–33]. Morphological characteristics and typical CC vary greatly in leaves of these crops and are presented in Table 1 [34].

Table 1. Morphological characteristics and typical CC of the inspected leaves.

Crop	Plant Functional Type	Length of Leaf Blade, mm	Width of Leaf Blade, mm	Form of Leaf Blade	Cover of Leaf Blade	Pubescence	Leaf Venation	CC, mg/L
<i>Triticum aestivum</i>	Annual	<300	10–20	Lanceolar	Smooth, scabrous	No	Parallel	3.9–9.9
<i>Betula populifolia</i>	Drought deciduous	50–70	40–60	Oval	Smooth, scabrous	Yes	Pinnate, dictyodromous	3.5–13.2
<i>Hordeum vulgare</i>	Annual	<300	20–30	Lanceolar	Smooth, scabrous	No	Parallel	4.2–9.9
<i>Ribes rubrum</i>	Drought deciduous	20–50	<120	Lobar-digitate	Smooth, scabrous	Yes	Dictyodromous	9.8–16.1
<i>Prunus padus</i>	Drought deciduous	60–130	35–60	Oval-lanceolar	Smooth, scabrous	Yes	Pinnate	1.7–5.5
<i>Hibiscus rosa-sinensis</i>	Evergreen perennial	50–120	30–85	Oval-digitate	Smooth, glossy	No	Dictyodromous	7.8–39.2

Leaves were cut at their growth point of the plant stems by scissors in the areas uniform in color, density and phenological characteristics. Each sample weighed at least 3 g, excluding stems and ears. The collected plants were packed in foil and zip bags for transportation.

The leaves of hibiscus, birch, bird-cherry tree and currant were collected in the Baibaki village located in the northeast of the Moscow region from April to June 2023. The climate there is humid continental with warm summers. The textural horizon of soddy-podzolic soils, the densest in profile, is brown, often with a yellowish or reddish tint. The reaction of soils is most often acidic throughout the profile, but neutral is possible in the lower, sometimes in the middle, parts of the profile in the presence of inherited carbonates. The humus content is 1.5–6% in the humus and 0.2–0.5% in the textural horizons.

Wheat and barley fields were located in the vicinity of the village Lobanovo in Perm Krai in July 2023. In terms of the climate, the land, being situated within a temperate continental climate zone, generally experiences short and moderately warm summers with a large amount of precipitation (472 mm per year). Soil there is soddy-podzolic loamy, characterized by a high content of nitrogen and phosphorus. Hydrolytic acidity is low, with 2.5–3.1 meq/100 g of soil in the upper horizon. The degree of saturation is about 88%, and pH value of the soil is 4.96. The topsoil contains 2.45–5.75% humus.

For wheat, samples with a significant variation in CC from four plots with different levels of fertility were included. Plants from these plots differed in health status and therefore had different CC in the leaves. The rest of the samples within this crop had no differences in leaf phenology, signs of disease and plant stress.

Each crop is represented by 15 samples. Their developmental stages as well as collection dates and location are presented in Table 2.

Table 2. Data on inspected leaf samples.

Crop	Collection Point	Collection Date	Developmental Stage	Soil Type	Conditions	Organic Material, %	P ₂ O ₅ , mg/kg	K ₂ O, mg/kg
<i>Triticum aestivum</i>	57.775713, 56.329550	7 May 2023	Mature			2.9	2.45–5.75	9–40.95
<i>Betula populifolia</i>	55.954216, 37.944919	11 May 2023	Mature			3.5	10.15	52.67
<i>Hordeum vulgare</i>	57.837534, 56.302138	9 May 2023	Mature	Sod-podzolic	Field	2.43	1.633	38.73
<i>Ribes rubrum</i>	55.953855, 37.944774	11 May 2023	Expanding			4	16.34	57.14
<i>Prunus padus</i>	55.951942, 37.943452	19 May 2023	Mature			3.5	10.15	52.67
<i>Hibiscus rosa-sinensis</i>	55.942252, 37.951099	19 May 2023	Senescing	Artificial soil	Laboratory	10	30	100

2.2. Experimental Protocol

Figure 2 illustrates the main stages of the experimental protocol. It includes plant collecting, reference measurements, HSI data acquisition, processing and analysis, choosing the best CI and building a multi-crop Chl model. Each sample was separated into a ratio of 1:3. One third of the leaves were used for reference spectrophotometric CC measurements and two thirds for hyperspectral data acquisition by HSI system.

The imager is based on a tandem AOTF, i.e., two identical wide-aperture non-collinear AO TeO₂ crystals deployed 180° in the diffraction plane with three polarizers placed in front of, between and behind them [35]. Polarization directions of the first and the last polarizers are parallel and are crossed with respect to the intermediate polarizer. Incident light passes through the front polarizer and then only its part with wavelength λ , which corresponds to the exact Bragg condition, diffracts on the volume grating created in the first AO crystal by an acoustic wave with a frequency f and changes the orientation of the polarization. Non-diffracted radiation of other wavelengths passes through the crystal and is cut by the second (intermediate) polarizer. Similarly, the radiation is filtered in the second AO crystal and the output polarizer and is then focused by the lens on the sensor of a monochrome camera for image acquisition and processing. The selected wavelength λ is driven by the frequency f of the PC-controlled high-frequency generator producing signals that are fed to

the AO crystals. By varying the f of the acoustic waves, a period of the diffraction grating can be tuned in order to obtain a spectral image on a particular wavelength $\lambda = v\Delta n/f$ (v —phase velocity of ultrasound, $\Delta n = n_e - n_o$ —birefringence of the crystal). Tandem AO filtration is necessary to avoid image aberrations and wavelength-dependent image drift introduced by AO diffraction in a single crystal. Thus, such an imager allows fast and arbitrary spectral access in a wide wavelength range of 450–850 nm. Table 3 shows the detailed specifications of the imager.

Table 3. AO imager technical characteristics.

Parameter	Value
Spectral tuning range, nm	450–850
Tuning time, μ s	10
Accuracy of spectral access, nm	0.1
Spectral resolution, nm	3.5 nm (at 532 nm)
Spatial resolution, pixels	500 × 500
Field of view, °	15 × 20
Working distance, m	1 – ∞
Frame rate	up to 100 images/s

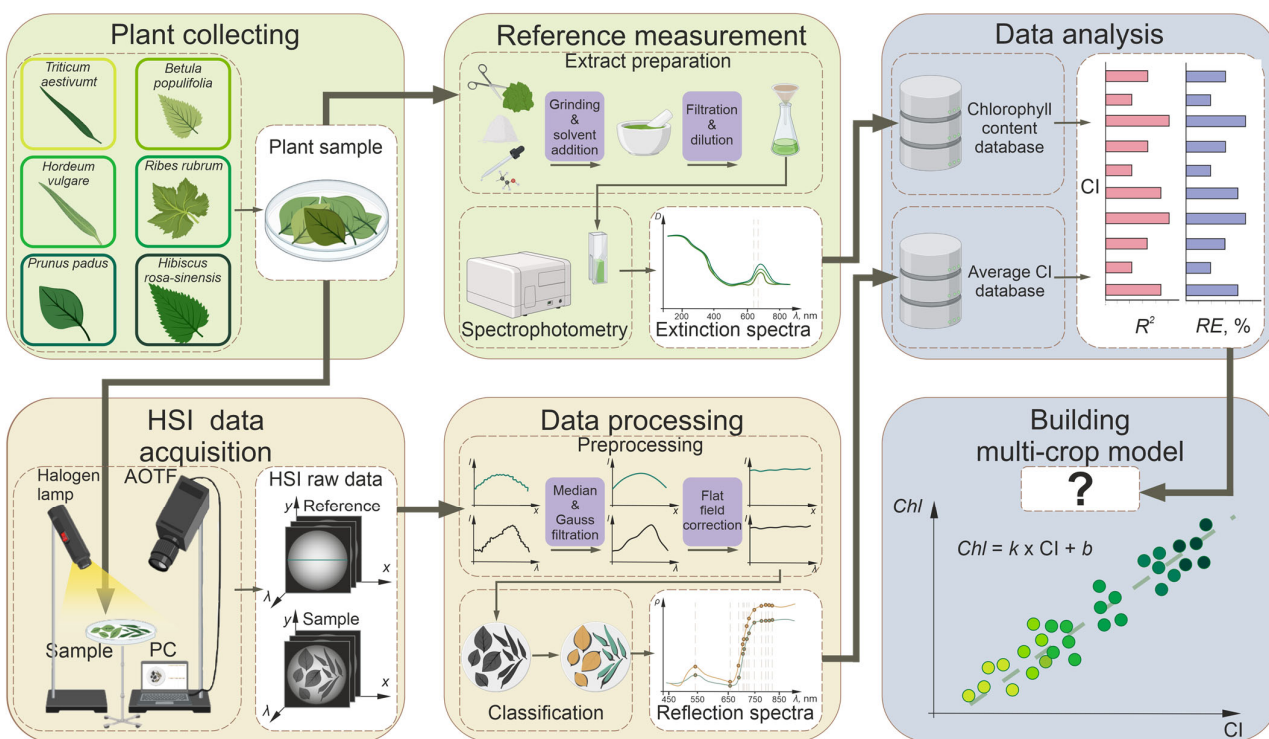


Figure 2. Experimental protocol.

During the experiments, the leaves were placed in a white uniform plate with reflectivity close to 1. For data correction necessary to compensate illumination non-uniformity, wavelength-dependent transmission of optical components and quantum efficiency of the sensor, the procedure described in [30] was applied.

Preprocessing of spectral images included the elimination of high-frequency noise and evaluation the spectral reflectivity. To reduce noise, median filtering was applied, and then spectral characteristics were smoothed using Gaussian function. The median filter operates on a 3-by-3 neighborhood centered around each pixel in the input image, while the Gaussian smoothing employs a 5-element sliding window. To counteract the influences of non-uniform leaf illumination and sensor sensitivity, wavelength-dependent AO diffraction efficiency, optical vignetting and the dependence of the transmittance

coefficient on the angle, we corrected the data using a flat field correction method [36]. The procedure involved filling the spectrometer's field of view with a test object characterized by both spatially and spectrally uniform reflectance. During calibration, the test chart was positioned at the same distance as the inspected leaves. The leaves in the images were detected via windowed binarization of the spectral angle map [37]. By averaging all pixels of the same class, the average reflection spectrum of each sample was determined.

For spectrophotometric analysis, a standard procedure based on solvent extraction using ethanol was applied. The average values of optical density at wavelengths of 649 and 665 nm for three extracts from one sample were used to calculate CC according to the formulas introduced by Wintermans and De Mots [38]. Table 4 contains measured CC values for all 6 crops.

Table 4. CC values obtained via spectrophotometric measurement.

Crop	Reference CC, mg/L
<i>Triticum aestivum</i>	6.50 ± 2.45
<i>Betula populifolia</i>	8.64 ± 1.69
<i>Hordeum vulgare</i>	9.12 ± 1.86
<i>Ribes rubrum</i>	10.67 ± 1.18
<i>Prunus padus</i>	16.83 ± 2.17
<i>Hibiscus rosa-sinensis</i>	25.49 ± 2.19

2.3. Selection of Spectral Bands

To avoid data redundancy, 10 of the most popular CIs were selected, and spectral images were acquired only at 11 wavelengths involved in these indices. Definitions of these CIs, as well as the crops reported suitable for them, and reference sources are listed in Table 5.

Table 5. Description of selected CIs.

Chlorophyll Index	Definition	Inspected Crops	Reference
Red-Edge Chlorophyll Index	$CI_{RE} = \frac{R_{760}}{R_{710}} - 1$	Maize, soybean	[39]
Modified Simple Ratio	$MSR_{705} = \frac{(R_{750}/R_{705})-1}{\sqrt{(R_{750}/R_{705})+1}}$	Winter wheat, eared, no-eared corn	[40]
MERIS terrestrial chlorophyll index	$MTCI = \frac{(R_{NIR}-R_{705})}{(R_{705}+R_{660})}$	Fir, maple	[41]
Modified Chlorophyll Absorption Ratio Index	$MCARI = [(R_{750} - R_{705}) - 0.2 \cdot (R_{750} - R_{550})] \cdot \left(\frac{R_{750}}{R_{705}}\right)$	Winter wheat, eared and no-eared corn	[40]
$\frac{MCARI}{OSAVI}$	$\frac{3 \cdot [(R_{750}-R_{705}) - 0.2 \cdot (R_{750}-R_{550}) \cdot \left(\frac{R_{750}}{R_{705}}\right)]}{(1+0.16) \cdot (R_{750}-R_{705}) \cdot (R_{750}+R_{705}+0.16)}$	Winter wheat, eared and no-eared corn	[40]
Normalized Difference Vegetation Index	$ND_{705} = \frac{(R_{750}-R_{705})}{(R_{750}+R_{705})}$	Herbaceous, sclerophyllous, succulent, grasses and others (53 species)	[42]
Optimized Soil-Adjusted Vegetation Index	$OSAVI = \frac{(1+0.16) \cdot (R_{750}-R_{705})}{(R_{750}+R_{705}+0.16)}$	Rice, woody plants, dense shrubs, cacti	[43,44]
Red-Edge Chlorophyll Absorption Index	$RECAI = \frac{(R_{800}-R_{720}) \cdot \left(\frac{R_{700}}{R_{550}}\right)}{R_{550}}$	Winter wheat, grape	[45,46]
Ratio spectral index	$RSI = \frac{R_{815}}{R_{704}}$	Rice, wheat, corn, soybean, sugar beet and grass	[47]
SR_{705}	$SR_{705} = \frac{R_{750}}{R_{705}}$	Herbaceous, sclerophyllous, succulent, grasses and others (53 species)	[42]

Figure 3 illustrates the positions of 11 wavelengths involved in 10 selected CIs and a typical plant spectrum. Image acquisition by AOTF-based imager at only these 11 wavelengths radically reduces data collection and processing time.

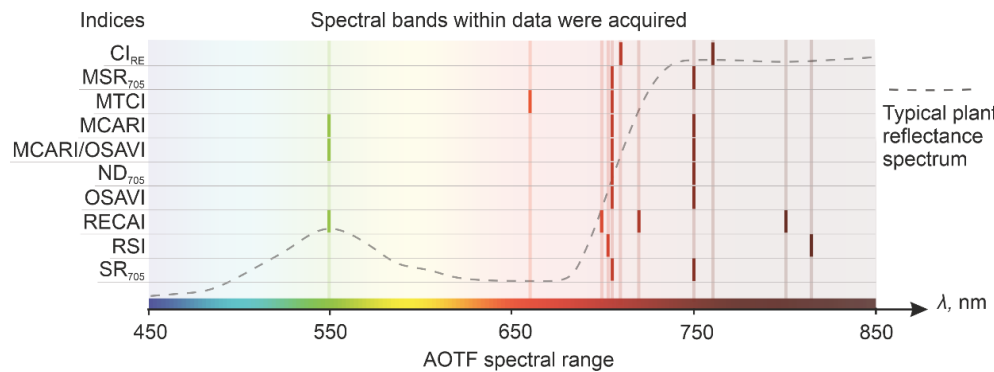


Figure 3. Spectral bands involved in selected CIs.

2.4. Model Evaluation

With reference CC and measured CIs, linear empirical models were built for each plant and their sets using the least squares method. To evaluate them, the coefficient of determination R^2 and the relative error RE were used. These statistical parameters were calculated using CC values determined from HSI spectrophotometric measurements as follows:

$$R^2 = 1 - \frac{\sum_{i=1}^n (CC_i - \bar{CC})^2}{\sum_{i=1}^n (CC_i - \bar{CC})}, \quad (1)$$

$$= \left[\frac{1}{n} \sum_{i=1}^n \frac{|CC_i - \bar{CC}|}{CC_i} \right] \cdot 100\%, \quad (2)$$

where \bar{CC} is the average value of the reference CC in the samples, and n is the total number of samples included in the model. The maximal R^2 and minimal RE correspond to the most reliable model for a given set of samples.

3. Results

3.1. Single-Crop Models

Based on reference CC values for each individual crop, linear models $Chl = k \cdot CI + b$ were built for 10 selected indices averaged over the sample area. Among these models, the most effective CIs in terms of CC accuracy were selected according to the maximum correlation and the minimum relative error (Figure 4). Only the model for *Triticum aestivum* showed a high coefficient of determination of 0.88 due to a significant spread in CC values within the selected leaves. Other crops have less CC variety among the samples and thus lower correlation and lower relative error RE . This means that the models optimal for these particular samples might be unsuitable for other CC ranges even in the same crops, e.g., at different growth stages, with disease or under stress.

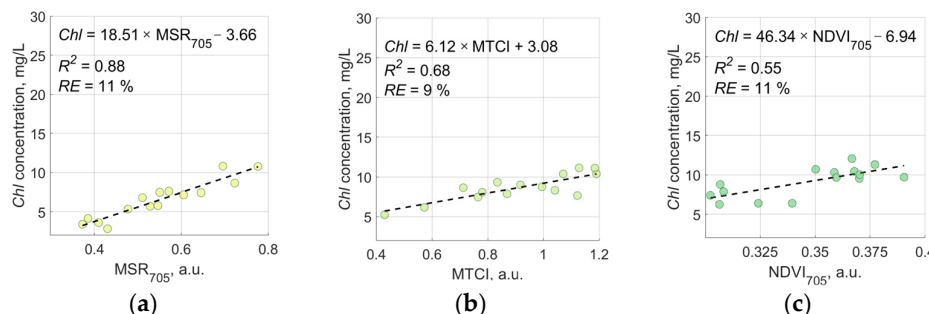


Figure 4. Cont.

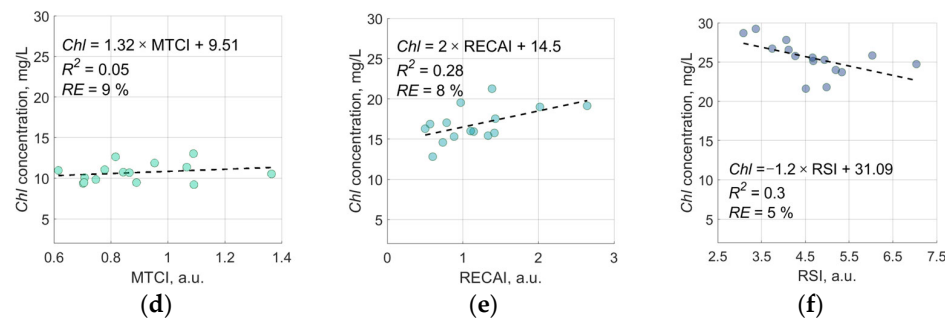


Figure 4. Individual crop models: (a) *Triticum aestivum*; (b) *Betula populifolia*; (c) *Hordeum vulgare*; (d) *Ribes rubrum*; (e) *Prunus padus*; (f) *Hibiscus rosa-sinensis*.

3.2. Multi-Crop Model

To build a multi-crop model that is well suited to all inspected plants, all 90 samples were included in our calculations, and all 10 selected CIs were tried. Values of R^2 and RE values for models based on these indices are presented in Figure 5a. MSR_{705} showed the highest determination coefficient at 0.89 and the lowest relative error at 15%. That is why this index was chosen as the most suitable one for specific crops and specific conditions of our experiment. It should be noticed that MSR_{705} is a two-wavelength (705 nm and 750 nm) index well established for wheat [40], and it really turned out to be the best choice for wheat (*Triticum aestivum*) but not for other single crops (Figure 4).

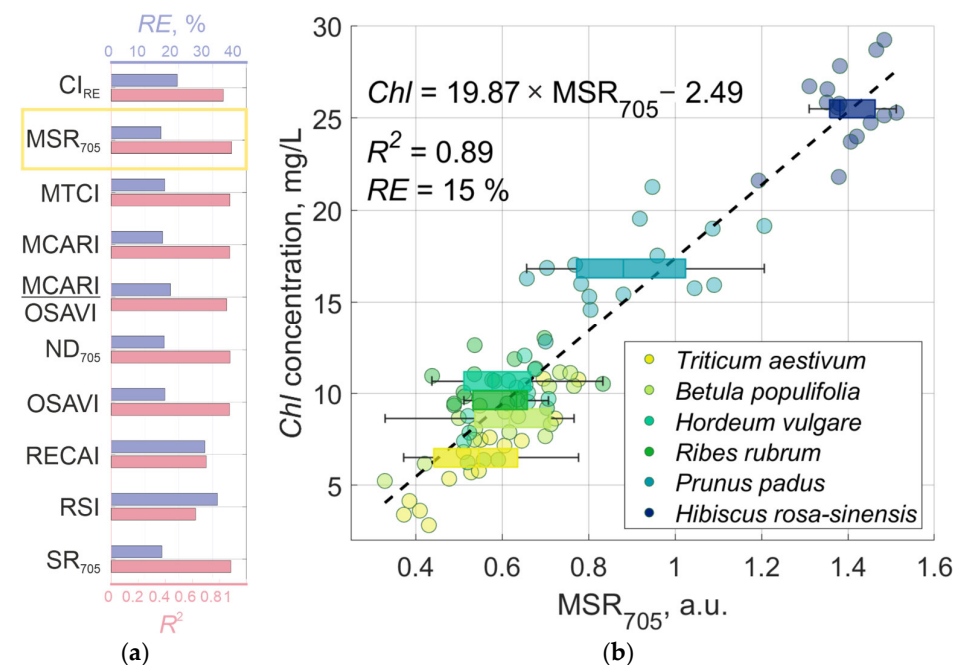


Figure 5. R^2 and RE values for the multi-crop model based on 10 different CIs (a) and the optimal MSR_{705} -based CC model (b).

Figure 5b shows the data point distribution in the CC- MSR_{705} space and the calculated MSR_{705} -based linear CC model. On each box, the central mark indicates the median, and the bottom and top edges indicate the 25th and 75th percentiles, respectively. The whiskers extend to the most extreme data points not considered outliers. It can be seen that the points of individual crops do not lie on this line, but in a wide CC range (4–27 mg/L) this line fits well with the whole amount of data points.

The average absolute errors between model-predicted chlorophyll content and actual detection data for *Triticum aestivum* are 1.36 mg/L, *Betula populifolia*—1.50 mg/L, *Hordeum*

vulgare—1.01 mg/L, *Ribes rubrum*—2.70 mg/L, *Prunus padus*—2.88 mg/L and *Hibiscus rosa-sinensis*—1.95 mg/L.

In this study, we tried to select crops that differ greatly in their physiological features and chlorophyll content, i.e., imitate the worst-case scenario. In practice, the model may be updated periodically by re-calibration, but in everyday practice (between calibrations) it works fine. We explored the efficiency of linear and various non-linear (power, exponential, polynomial and logarithmic) regression methods, compared them and summarized the results in Table 6. It contains the most effective index, coefficient of determination R^2 and relative error RE for each type of regression. The univariate linear regression model was built with CC as the dependent variable and vegetation indices as independent variables. Four vegetation indices including MSR_{705} , $NDVI_{705}$ and SR_{705} with the best fit were selected as independent variables to construct the multiple linear regression model. Table 6 indicates that non-linear regression and incorporating a combination of indices did not yield any improvement in the results.

Table 6. Efficiency of various regression models.

Regression Type	Regression Model	R^2	$RE, \%$
Linear	$Chl = 19.87 \times MSR_{705} - 2.49$	0.89	15
Polynomial ($n = 2$)	$Chl = 54.82 \times (NDVI_{705})^2 + 6.34 \times NDVI_{705} + 0.72$	0.89	14.46
Polynomial ($n = 3$)	$Chl = -0.17 \times (NDVI_{705})^3 + 0.54 \times (NDVI_{705})^2 + 9.18 \times NDVI_{705} - 10.26$	0.89	14.41
Power	$Chl = 17.15 \times (MSR_{705})^{1.17}$	0.89	14.46
Exponential	$Chl = 2.66 \times \exp(3.68 \times NDVI_{705})$	0.89	14.91
Logarithmic	$Chl = 21.69 \times \exp(0.75 \times SR_{705})$	0.89	14.57
Multiple linear	$Chl = 18.99 + 102.53 \times MSR_{705} - 94.34 \times NDVI_{705} - 18.91 \times SR_{705}$	0.89	14.44
	$Chl = -2.65 + 19.41 \times MSR_{705} + 1.30 \times NDVI_{705}$	0.89	14.55
	$Chl = -7.72 + 23.90 \times NDVI_{705} + 4.38 \times SR_{705}$	0.89	14.57

To provide more comprehensive data on the efficiency of the various CIs, we also calculated mean and RMS values obtained when they were introduced in the single-crop and multi-crop models (Appendix A).

3.3. Chlorophyll Mapping

With spectral images obtained at the wavelengths 705 nm and 750 nm, MSR_{705} maps were built for each crop. Then, applying a multi-crop model to each pixel of these maps, CC maps were calculated. Figure 6 illustrates this pipeline for the images of the plate filled with leaves of *Prunus padus* and *Hibiscus rosa-sinensis*.

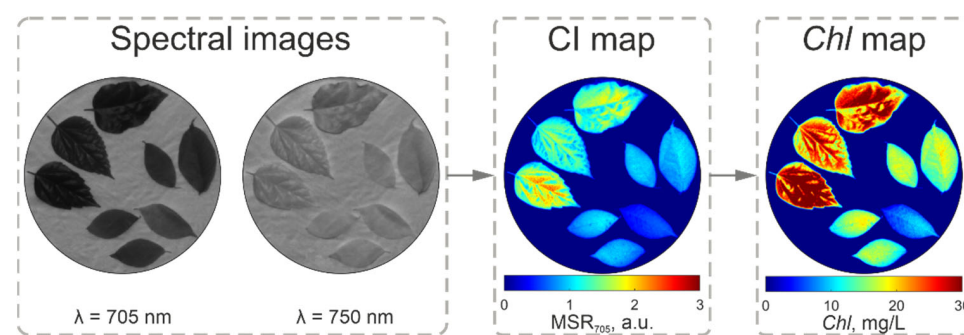


Figure 6. CC mapping pipeline.

This processing pipeline was applied for all 90 plant samples. Figure 7 shows examples of the calculated chlorophyll maps. For ease of comparison, all maps are displayed in the same chlorophyll range (0–30 mg/L).

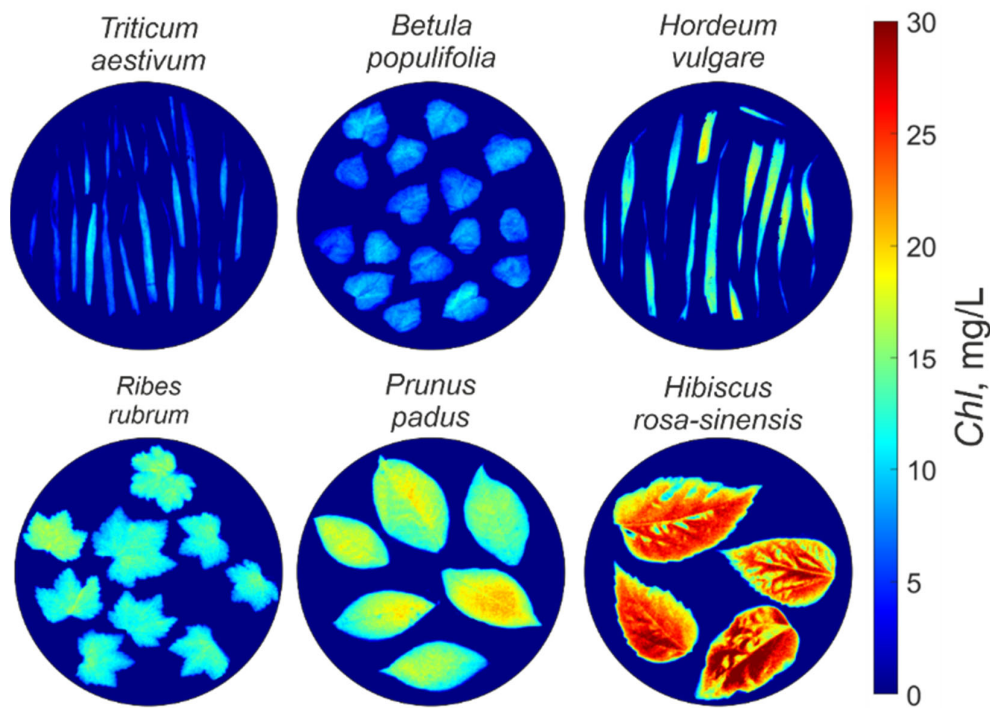


Figure 7. CC maps of 6 studied crops.

4. Discussion

Leaf chemical properties are the principal predictors of plant physiology and inner biochemical processes such as photosynthesis [48], and they also indicate seasonal changes in the availability of water and nutrients [49]. Being primary photosynthetic pigments, chlorophylls interact with sunlight and respond to various environmental stressors [50]. Therefore, accurate CC monitoring is one of the key procedures in modern PA. The solution to this task is much more complicated when multiple different crops are observed simultaneously and a single CI has to be found to calculate CC within the whole field of view. As some studies indicate a decline in the effectiveness of certain radiative transfer models in multi-crop studies [51,52], along with challenges in the accuracy of inversion and the complexity of CC map calculation at high spatial resolution, we chose a well-proven empirical method for CC assessment. To reduce the impact of lighting and observation conditions on the obtained data, as well as correct distortions introduced by the imager, we developed an algorithm for AO imager calibration and spatio-spectral data correction. In this study, we demonstrated the applicability of AO imagery to multi-crop CC mapping, but a few questions related to practical implementation of this approach remain open.

First, to build a reliable linear regression model suitable for multiple crops, it is necessary to analyze samples with the widest possible variety of CC (Figure 5b). In practice, the selection of plants of different type and developmental stages to ensure a wide CC range, e.g., 5–30 mg/L, may be laborious and time-consuming. Moreover, the regression model has to be verified periodically and refined if necessary due to the change in the growth stage, presence of environmental stressors and other factors.

Second, accuracy of CC evaluation largely depends on the number of inspected samples. Each of them should be supported by well-established routine Chl concentration measurements. Even with 90 samples analyzed in this study, it cannot be guaranteed that the obtained determination coefficient of 0.89 and relative error of 15% are valid for the plants not included in this study due to other morphological and physiological properties.

This means that with every new sample the model will change a bit and become more precise. So, a robust CC evaluation needs a regular update of the model with respect to the properties of studied crops.

Third, reliable CC mapping requires precise spatio-spectral calibration of the AO imager with respect to image distortions, wavelength-dependent transmission of the optical transmittance, vignetting, quantum efficiency of the sensor and other factors. In laboratory conditions, this can be implemented by deployment of a stable mechanical stand and calibration data acquisition using a few certified light sources and test charts [53,54].

With these circumstances taken into account, we believe that the proposed approach may become an effective tool for fast and non-contact CC mapping, which may to a large extent substitute time-consuming and laborious spectrophotometric, chromatographic and other procedures. In this study, we chose the crops that differ greatly in physiological properties and Chl content in order to show how, in this case, a proper index and regression model may be found using an AO imaging system. The right choice of index and model depends on the number and features of the inspected crops. Therefore, the strategy for data collection has to include as complete a variety of crops as possible. Once it is known what crops may be in the field, the technique presented in this study can be applied to define the best index and regression model in terms of accuracy with respect to a multi-crop scene. The fewer the crops, the more accurate these initial CC measurements will be. As the growth phase change and environmental stressors appear, verification of the optimal CC and regression model makes sense. Thus, we can recommend a periodic collection of the samples with the widest possible variety of CC at the moment and applying the presented data processing pipeline to define if CC has to be revised and if the regression model needs refinement.

5. Conclusions

The CI-based concept is a dominating approach to remote CC mapping. Up to now, there has been no standard and universal CI that suits well to all plants at any conditions. Thus, it is always necessary to define the optimal CI and then carry out routine CC measurements. This feasibility, six-crop study demonstrates that AO imagery delivers all the necessary features (rapid and fast random-access tuning, high image quality, etc.) to solve this task in the most efficient way, at least in laboratory conditions, and become a fast and non-contact alternative for the replacement of time-consuming and non-imaging spectrophotometric CC measurements.

With the AOTF-based imager, spectral images were acquired at only 11 wavelengths involved in 10 of the most popular CIs, CC linear regression models were built based on each of these indices and the optimal one was chosen for all inspected plants in terms of accuracy. This strategy allows fast data acquisition and processing, selection of the most suitable CI and building a reliable multi-crop CC model.

The results of this study demonstrate that acousto-optic imagery shows great promise for fast chlorophyll content assessment and other laboratory spectral-index-based measurements.

Author Contributions: Conceptualization, A.M.; methodology, A.Z., A.G. and A.M.; data curation, V.G., A.K., K.D., G.N., D.F. and S.P.; software, A.Z.; validation, V.G., A.G. and D.F.; investigation, A.G., V.G., A.Z. and D.F.; resources, A.M. and A.G.; writing—original draft preparation, A.M., A.Z. and A.G.; writing—review and editing, A.G., V.G., S.P. and V.P.; visualization, A.Z.; supervision, A.M.; project administration, A.M. and A.G.; funding acquisition, A.M. and A.G. All authors have read and agreed to the published version of the manuscript.

Funding: This research was supported by the Ministry of Science and Higher Education of the Russian Federation, the Priority 2030 program, the Bauman GoGreen strategic project, the PRI-OR/SN/NU/22/SP1/7 project. The experimental setup and image acquisition software were developed within Federal State Task Program of Scientific and Technological Centre of Unique Instrumentation of the Russian Academy of Sciences (project #FFNS-2022-0010).

Data Availability Statement: The datasets generated during the current study are available from the corresponding author on reasonable request.

Acknowledgments: The results were obtained using the equipment of the Centre for Collective Use of the Scientific and Technological Centre for Unique Instrumentation of the Russian Academy of Sciences [456451, <https://ckp.ntcup.ru>]. Figures 1 and 2 were created with BioRender.com.

Conflicts of Interest: The authors declare no conflicts of interest.

Appendix A

Table A1. Values of each chlorophyll index in single-crop models and multi-crop models.

Crop	<i>Triticum aestivum</i>	<i>Betula populifolia</i>	<i>Hordeum vulgare</i>	<i>Ribes rubrum</i>	<i>Prunus padus</i>	<i>Hibiscus rosa-sinensis</i>	Multi-Crop
CI _{RE}	0.86 ± 0.63	0.75 ± 0.57	0.78 ± 0.3	0.71 ± 0.51	1.18 ± 0.8	2.19 ± 0.45	1.08 ± 1.67
MSR ₇₀₅	0.55 ± 0.37	0.61 ± 0.39	0.61 ± 0.2	0.59 ± 0.32	0.89 ± 0.49	1.4 ± 0.24	0.77 ± 0.97
MTCI	0.82 ± 0.83	0.91 ± 0.68	0.85 ± 0.36	0.88 ± 0.6	1.56 ± 1.29	2.63 ± 0.75	1.27 ± 2.13
MCARI	0.56 ± 0.53	0.7 ± 0.57	0.77 ± 0.28	0.66 ± 0.51	1.18 ± 0.9	2.13 ± 0.71	1 ± 1.74
MCARI _{OSAVI}	1.67 ± 0.75	1.94 ± 0.7	2.12 ± 0.27	1.87 ± 0.63	2.48 ± 0.95	3.43 ± 0.81	2.25 ± 1.89
ND ₇₀₅	0.32 ± 0.17	0.34 ± 0.18	0.35 ± 0.09	0.34 ± 0.14	0.46 ± 0.18	0.61 ± 0.06	0.4 ± 0.35
OSAVI	0.33 ± 0.17	0.36 ± 0.18	0.36 ± 0.09	0.35 ± 0.14	0.47 ± 0.18	0.62 ± 0.07	0.41 ± 0.34
RECAI	0.92 ± 0.75	0.47 ± 0.7	0.45 ± 0.4	0.33 ± 0.57	1.17 ± 1.74	2.73 ± 1.36	1.01 ± 2.68
RSI	2.30 ± 1.06	2.22 ± 1.3	1.95 ± 0.96	1.91 ± 0.95	3.19 ± 2.74	4.67 ± 3.03	2.71 ± 3.46
SR ₇₀₅	1.95 ± 0.77	2.07 ± 0.8	2.07 ± 0.41	2.03 ± 0.68	2.73 ± 1.26	4.18 ± 0.78	2.51 ± 2.52

References

- Rockström, J.; Williams, J.; Daily, G.; Noble, A.; Matthews, N.; Gordon, L.; Wetterstrand, H.; DeClerck, F.; Shah, M.; Steduto, P.; et al. Sustainable Intensification of Agriculture for Human Prosperity and Global Sustainability. *Ambio* **2017**, *46*, 4–17. [[CrossRef](#)]
- Hunter, M.C.; Smith, R.G.; Schipanski, M.E.; Atwood, L.W.; Mortensen, D.A. Agriculture in 2050: Recalibrating Targets for Sustainable Intensification. *Bioscience* **2017**, *67*, 386–391. [[CrossRef](#)]
- Gebbers, R.; Adamchuk, V.I. Precision Agriculture and Food Security. *Science* **2010**, *327*, 828–831. [[CrossRef](#)]
- Majumdar, J.; Naraseeyappa, S.; Ankalaki, S. Analysis of Agriculture Data Using Data Mining Techniques: Application of Big Data. *J. Big Data* **2017**, *4*, 20. [[CrossRef](#)]
- Féret, J.B.; Gitelson, A.A.; Noble, S.D.; Jacquemoud, S. PROSPECT-D: Towards Modeling Leaf Optical Properties through a Complete Lifecycle. *Remote Sens. Environ.* **2017**, *193*, 204–215. [[CrossRef](#)]
- Roper, J.M.; Garcia, J.F.; Tsutsui, H. Emerging Technologies for Monitoring Plant Health in Vivo. *ACS Omega* **2021**, *6*, 5101–5107. [[CrossRef](#)] [[PubMed](#)]
- Barbedo, J.G.A. A Review on the Use of Unmanned Aerial Vehicles and Imaging Sensors for Monitoring and Assessing Plant Stresses. *Drones* **2019**, *3*, 40. [[CrossRef](#)]
- Gitelson, A.A.; Peng, Y.; Arkebauer, T.J.; Schepers, J. Relationships between Gross Primary Production, Green LAI, and Canopy Chlorophyll Content in Maize: Implications for Remote Sensing of Primary Production. *Remote Sens. Environ.* **2014**, *144*, 65–72. [[CrossRef](#)]
- Benelli, A.; Cevoli, C.; Fabbri, A. In-Field Hyperspectral Imaging: An Overview on the Ground-Based Applications in Agriculture. *J. Agric. Eng.* **2020**, *51*, 129–139. [[CrossRef](#)]
- Lu, B.; Dao, P.D.; Liu, J.; He, Y.; Shang, J. Recent Advances of Hyperspectral Imaging Technology and Applications in Agriculture. *Remote Sens.* **2020**, *12*, 2659. [[CrossRef](#)]
- Mulla, D.J. Twenty Five Years of Remote Sensing in Precision Agriculture: Key Advances and Remaining Knowledge Gaps. *Biosyst. Eng.* **2013**, *114*, 358–371. [[CrossRef](#)]
- Kwan, C. Remote Sensing Performance Enhancement in Hyperspectral Images. *Sensors* **2018**, *18*, 3598. [[CrossRef](#)]
- Sethy, P.K.; Pandey, C.; Sahu, Y.K.; Behera, S.K. Hyperspectral Imagery Applications for Precision Agriculture—A Systemic Survey. *Multimed. Tools Appl.* **2021**, *81*, 3005–3038. [[CrossRef](#)]
- Li, P.; Wang, Q. Retrieval of Chlorophyll for Assimilating Branches of a Typical Desert Plant through Inversed Radiative Transfer Models. *Int. J. Remote Sens.* **2013**, *34*, 2402–2416. [[CrossRef](#)]
- Vohland, M.; Jarmer, T. Estimating Structural and Biochemical Parameters for Grassland from Spectroradiometer Data by Radiative Transfer Modelling (PROSPECT+SAIL). *Int. J. Remote Sens.* **2008**, *29*, 191–209. [[CrossRef](#)]
- Sehgal, V.K.; Chakraborty, D.; Sahoo, R.N. Inversion of Radiative Transfer Model for Retrieval of Wheat Biophysical Parameters from Broadband Reflectance Measurements. *Inf. Process. Agric.* **2016**, *3*, 107–118. [[CrossRef](#)]

17. Cheng, J.; Yang, H.; Qi, J.; Sun, Z.; Han, S.; Feng, H.; Jiang, J.; Xu, W.; Li, Z.; Yang, G.; et al. Estimating Canopy-Scale Chlorophyll Content in Apple Orchards Using a 3D Radiative Transfer Model and UAV Multispectral Imagery. *Comput. Electron. Agric.* **2022**, *202*, 107401. [[CrossRef](#)]
18. Berger, K.; Verrelst, J.; Féret, J.B.; Hank, T.; Wocher, M.; Camps-Valls, G. Retrieval of Aboveground Crop Nitrogen Content with a Hybrid Machine Learning Method. *Int. J. Appl. Earth Obs. Geoinf.* **2020**, *92*, 102174. [[CrossRef](#)]
19. Verrelst, J.; Camps-Valls, G.; Muñoz-Marí, J.; Rivera, J.P.; Veroustraete, F.; Clevers, J.G.P.W.; Moreno, J. Optical Remote Sensing and the Retrieval of Terrestrial Vegetation Bio-Geophysical Properties—A Review. *ISPRS J. Photogramm. Remote Sens.* **2015**, *108*, 273–290. [[CrossRef](#)]
20. Lu, B.; He, Y. Evaluating Empirical Regression, Machine Learning, and Radiative Transfer Modelling for Estimating Vegetation Chlorophyll Content Using Bi-Seasonal Hyperspectral Images. *Remote Sens.* **2019**, *11*, 1979. [[CrossRef](#)]
21. Li, J.; Wijewardane, N.K.; Ge, Y.; Shi, Y. Improved Chlorophyll and Water Content Estimations at Leaf Level with a Hybrid Radiative Transfer and Machine Learning Model. *Comput. Electron. Agric.* **2023**, *206*, 107669. [[CrossRef](#)]
22. Haboudane, D.; Miller, J.R.; Tremblay, N.; Zarco-Tejada, P.J.; Dextraze, L. Integrated Narrow-Band Vegetation Indices for Prediction of Crop Chlorophyll Content for Application to Precision Agriculture. *Remote Sens. Environ.* **2002**, *81*, 416–426. [[CrossRef](#)]
23. Zeng, Y.; Hao, D.; Huete, A.; Dechant, B.; Berry, J.; Chen, J.M.; Joiner, J.; Frankenberg, C.; Bond-Lamberty, B.; Ryu, Y.; et al. Optical Vegetation Indices for Monitoring Terrestrial Ecosystems Globally. *Nat. Rev. Earth Environ.* **2022**, *3*, 477–493. [[CrossRef](#)]
24. Bannari, A.; Morin, D.; Bonn, F.; Huete, A.R. A Review of Vegetation Indices. *Remote Sens. Rev.* **1995**, *13*, 95–120. [[CrossRef](#)]
25. Ma, Y.; Zhang, Q.; Yi, X.; Ma, L.; Zhang, L.; Huang, C.; Zhang, Z.; Lv, X. Estimation of Cotton Leaf Area Index (LAI) Based on Spectral Transformation and Vegetation Index. *Remote Sens.* **2021**, *14*, 136. [[CrossRef](#)]
26. Inoue, Y.; Penueles, J.; Nouevillon, Y.; Moran, M.S. Hyperspectral Reflectance Measurements for Estimating Eco-Physiological Status of Plants. In *Hyperspectral Remote Sensing of the Land and Atmosphere*; SPIE: Bellingham, WA, USA, 2001; Volume 4151, pp. 153–163. [[CrossRef](#)]
27. Inoue, Y.; Penueles, J. An AOTF-Based Hyperspectral Imaging System for Field Use in Ecophysiological and Agricultural Applications. *Int. J. Remote Sens.* **2010**, *22*, 3883–3888. [[CrossRef](#)]
28. Slovin, J.P.; Bandurski, R.S.; Cohen, J.D. Chapter 5 Auxin. *New Compr. Biochem.* **1999**, *33*, 115–140. [[CrossRef](#)]
29. Calpe-Maravilla, J.; Vila-Frances, J.; Ribes-Gomez, E.; Duran-Bosch, V.; Munoz-Mari, J.; Amoros-Lopez, J.; Gomez-Chova, L.; Tajahuerce-Romera, E. 400- to 1000-Nm Imaging Spectrometer Based on Acousto-Optic Tunable Filters. In *Sensors, Systems, and Next-Generation Satellites VIII*; SPIE: Bellingham, WA, USA, 2004; Volume 5570, p. 460. [[CrossRef](#)]
30. Zolotukhina, A.; Machikhin, A.; Guryleva, A.; Gresis, V.; Tedeeva, V. Extraction of Chlorophyll Concentration Maps from AOTF Hyperspectral Imagery. *Front. Environ. Sci.* **2023**, *11*, 480. [[CrossRef](#)]
31. Pyakurel, A.; Wang, J.R. Leaf Morphological Variation among Paper Birch (*Betula papyrifera* Marsh.) Genotypes across Canada. *Open J. Ecol.* **2013**, *03*, 284–295. [[CrossRef](#)]
32. Leather, S.R. *Prunus padus* L. *J. Ecol.* **1996**, *84*, 125. [[CrossRef](#)]
33. Siregar, A.Y.; Salamah, A. Variation of Leaf Morphology of Hibiscus Rosa-Sinensis L. under Various Light Intensities at Universitas Indonesia Campus Area and Citayam, Depok. In *IOP Conference Series: Earth and Environmental Science*; IOP Publishing: Bristol, UK, 2020; Volume 524. [[CrossRef](#)]
34. Chitwood, D.H.; Sinha, N.R. Evolutionary and Environmental Forces Sculpting Leaf Development. *Curr. Biol.* **2016**, *26*, R297–R306. [[CrossRef](#)] [[PubMed](#)]
35. Pustovoit, V.I.; Pozhar, V.E.; Mazur, M.M.; Shorin, V.N.; Kutuza, I.B.; Perchik, A.V. Double-AOTF Spectral Imaging System. In *Acousto-Optics and Photoacoustics*; SPIE: Bellingham, WA, USA, 2005; Volume 5953, pp. 200–203. [[CrossRef](#)]
36. Pu, R. *Hyperspectral Remote Sensing: Fundamentals and Practices*; CRC Press: Boca Raton, FL, USA, 2017; pp. 1–466.
37. Padma, S.; Sanjeevi, S. Jeffries Matusita-Spectral Angle Mapper (JM-SAM) Spectral Matching for Species Level Mapping at Bhitarkanika, Muthupet and Pichavaram Mangroves. *Int. Arch. Photogramm. Remote Sens. Spat. Inf. Sci.* **2014**, *XL–8*, 1403–1411. [[CrossRef](#)]
38. Wintermans, J.F.G.M.; De Mots, A. Spectrophotometric Characteristics of Chlorophylls a and b and Their Phenophytins in Ethanol. *Biochim. Biophys. Acta (BBA)—Biophys. Incl. Photosynth.* **1965**, *109*, 448–453. [[CrossRef](#)]
39. Gitelson, A.A.; Viña, A.; Ciganda, V.; Rundquist, D.C.; Arkebauer, T.J. Remote Estimation of Canopy Chlorophyll Content in Crops. *Geophys. Res. Lett.* **2005**, *32*, L08403. [[CrossRef](#)]
40. Wu, C.; Niu, Z.; Tang, Q.; Huang, W. Estimating Chlorophyll Content from Hyperspectral Vegetation Indices: Modeling and Validation. *Agric. For. Meteorol.* **2008**, *148*, 1230–1241. [[CrossRef](#)]
41. Dash, J.; Curran, P.J. The MERIS Terrestrial Chlorophyll Index. *Int. J. Remote Sens.* **2004**, *25*, 5403–5413. [[CrossRef](#)]
42. Sims, D.A.; Gamon, J.A. Relationships between Leaf Pigment Content and Spectral Reflectance across a Wide Range of Species, Leaf Structures and Developmental Stages. *Remote Sens. Environ.* **2002**, *81*, 337–354. [[CrossRef](#)]
43. Yuhalo, A.; Norasma, N.; Ya, C.; Roslin, A.; Ismail, M.R. SCIENCE & TECHNOLOGY Rice Chlorophyll Content Monitoring Using Vegetation Indices from Multispectral Aerial Imagery. *Pertanika J. Sci. Technol.* **2020**, *28*, 779–795.
44. Fern, R.R.; Foxley, E.A.; Bruno, A.; Morrison, M.L. Suitability of NDVI and OSAVI as Estimators of Green Biomass and Coverage in a Semi-Arid Rangeland. *Ecol. Indic.* **2018**, *94*, 16–21. [[CrossRef](#)]

45. Cui, B.; Zhao, Q.; Huang, W.; Song, X.; Ye, H.; Zhou, X. A New Integrated Vegetation Index for the Estimation of Winter Wheat Leaf Chlorophyll Content. *Remote Sens.* **2019**, *11*, 974. [[CrossRef](#)]
46. Laroche-Pinel, E.; Albughdadi, M.; Dutheoit, S.; Chéret, V.; Rousseau, J.; Clenet, H. Understanding Vine Hyperspectral Signature through Different Irrigation Plans: A First Step to Monitor Vineyard Water Status. *Remote Sens.* **2021**, *13*, 536. [[CrossRef](#)]
47. Inoue, Y.; Guérif, M.; Baret, F.; Skidmore, A.; Gitelson, A.; Schlerf, M.; Darvishzadeh, R.; Olioso, A. Simple and Robust Methods for Remote Sensing of Canopy Chlorophyll Content: A Comparative Analysis of Hyperspectral Data for Different Types of Vegetation. *Plant Cell Environ.* **2016**, *39*, 2609–2623. [[CrossRef](#)] [[PubMed](#)]
48. Evain, S.; Flexas, J.; Moya, I. A New Instrument for Passive Remote Sensing: 2. Measurement of Leaf and Canopy Reflectance Changes at 531 Nm and Their Relationship with Photosynthesis and Chlorophyll Fluorescence. *Remote Sens. Environ.* **2004**, *91*, 175–185. [[CrossRef](#)]
49. Gilman, E.L.; Ellison, J.; Duke, N.C.; Field, C. Threats to Mangroves from Climate Change and Adaptation Options: A Review. *Aquat. Bot.* **2008**, *89*, 237–250. [[CrossRef](#)]
50. Carter, G.A.; Knapp, A.K. Leaf Optical Properties in Higher Plants: Linking Spectral Characteristics to Stress and Chlorophyll Concentration. *Am. J. Bot.* **2001**, *88*, 677–684. [[CrossRef](#)] [[PubMed](#)]
51. Darvishzadeh, R.; Skidmore, A.; Schlerf, M.; Atzberger, C. Inversion of a Radiative Transfer Model for Estimating Vegetation LAI and Chlorophyll in a Heterogeneous Grassland. *Remote Sens. Environ.* **2008**, *112*, 2592–2604. [[CrossRef](#)]
52. Darvishzadeh, R.; Skidmore, A.; Schlerf, M.; Atzberger, C.; Corsi, F.; Cho, M. LAI and Chlorophyll Estimation for a Heterogeneous Grassland Using Hyperspectral Measurements. *ISPRS J. Photogramm. Remote Sens.* **2008**, *63*, 409–426. [[CrossRef](#)]
53. Katrašnik, J.; Bürmen, M.; Pernuš, F.; Likar, B. Spectral Characterization and Calibration of AOTF Spectrometers and Hyper-Spectral Imaging Systems. *Chemom. Intell. Lab. Syst.* **2010**, *101*, 23–29. [[CrossRef](#)]
54. Martynov, G.N.; Pozhar, V.E.; Gorevoy, A.V.; Machikhin, A.S. Spatirospectral Transformation of Noncollimated Light Beams Diffracted by Ultrasound in Birefringent Crystals. *Photonics Res.* **2021**, *9*, 687–693. [[CrossRef](#)]

Disclaimer/Publisher’s Note: The statements, opinions and data contained in all publications are solely those of the individual author(s) and contributor(s) and not of MDPI and/or the editor(s). MDPI and/or the editor(s) disclaim responsibility for any injury to people or property resulting from any ideas, methods, instructions or products referred to in the content.